Effect of bending buckling of carbon nanotubes on thermal conductivity of carbon nanotube materials

Alexey N. Volkov, Takuma Shiga, David Nicholson, Junichiro Shiomi, and Leonid V. Zhigilei

Citation: J. Appl. Phys. **111**, 053501 (2012); doi: 10.1063/1.3687943
View online: http://dx.doi.org/10.1063/1.3687943
View Table of Contents: http://jap.aip.org/resource/1/JAPIAU/v111/i5
Published by the American Institute of Physics.

Effect of bending buckling of carbon nanotubes on thermal conductivity of carbon nanotube materials

Alexey N. Volkov,[1] Takuma Shiga,[2] David Nicholson,[1] Junichiro Shiomi,[2,a)] and Leonid V. Zhigilei[1,a)]
[1]*University of Virginia, Department of Materials Science and Engineering, 395 McCormick Road, Charlottesville, Virginia 22904-4745, USA*
[2]*The University of Tokyo, Department of Mechanical Engineering, 7-3-1 Hongo, Bunkyo-ku, Tokyo 113-8656, Japan*

(Received 19 October 2011; accepted 28 January 2012; published online 1 March 2012)

The effect of bending buckling of carbon nanotubes (CNTs) on thermal conductivity of CNT materials is investigated in atomistic and mesoscopic simulations. Nonequilibrium molecular dynamics simulations of the thermal conductance through an individual buckling kink in a (10,10) single-walled CNT reveal a strong dependence (close to inverse proportionality) of the thermal conductance of the buckling kink on the buckling angle. The value of the buckling kink conductance divided by the cross-sectional area of the CNT ranges from 40 to 10 $GWm^{-2}K^{-1}$ as the buckling angle changes from 20 to 110°. The predictions of the atomistic simulations are used for parameterization of a mesoscopic model that enables calculations of thermal conductivity of films composed of thousands of CNTs arranged into continuous networks of bundles. The results of mesoscopic simulations demonstrate that the conductivity of CNT films is sensitive to the angular dependence of the buckling kink conductance and the length of the individual CNTs. For a film composed of 1 μm-long CNTs, the values of the in-plane film conductivity predicted with a constant conductance of 20 $GWm^{-2}K^{-1}$ and the angular-dependent conductance obtained in atomistic simulations are about 40 and 20% lower than the conductivity predicted for the same film with zero thermal resistance of the buckling kinks, respectively. The weaker impact of the angular-dependent buckling kink conductance on the effective conductivity of the film is explained by the presence of a large fraction of kinks that have small buckling angles and correspondingly large values of conductance. The results of the simulations suggest that the finite conductance of the buckling kinks has a moderate, but non-negligible, effect on thermal conductivity of materials composed of short CNTs with length up to 1 μm. The contribution of the buckling kink thermal resistance becomes stronger for materials composed of longer CNTs and/or characterized by higher density of buckling kinks. © *2012 American Institute of Physics*.
[http://dx.doi.org/10.1063/1.3687943]

I. INTRODUCTION

Individual carbon nanotubes (CNT) have exceptionally high thermal conductivity, with both theoretical calculations[1–5] and experimental measurements[6–9] predicting values from about 150 to 6600 $Wm^{-1}K^{-1}$ at 300 K. Measurements of thermal conductivity of CNT materials, such as CNT films, mats, buckypaper, and vertically aligned arrays, however, yield one to three orders of magnitude smaller values, in the range of 0.1–90 $Wm^{-1}K^{-1}$,[10–14] which increases up to ~220 $Wm^{-1}K^{-1}$ with increasing degree of alignment of CNTs.[10] It is generally accepted that the main factor that limits the thermal conductivity of CNT materials is the weak thermal coupling between the individual CNTs, manifesting itself in small contact conductance of CNT-CNT interfaces.[14–21] The contribution of other factors that may be responsible for the reduction of the effective conductivity of CNT materials, such as bending buckling[22] and defects of atomic structure of individual CNTs,[1,23] or presence of isotope impurities,[4] are much less explored and are not systematically quantified. In this paper, we use a combination of atomistic and mesoscopic computer modeling to investigate the effect of bending buckling of individual CNTs on thermal conductivity of CNT materials.

In CNT materials, individual CNTs are bound together by van der Waals forces[24] and form continuous networks of interconnected bundles.[25–29] Experimental observations[30,31] show that nanotubes in the CNT network structures are subjected to bending buckling. Recent mesoscopic simulations[32,33] provide a dynamic illustration of spontaneous self-organization of individual CNTs into networks of bundles and reveal that the bending buckling plays a major role in ensuring the structural integrity of the CNT films.[33] The bending buckling of a nanotube results in the formation of a localized buckling kink,[30,34] where the original cylindrical shape of the nanotube is highly distorted. The distortions result in modification of mechanical and thermal properties of the buckled nanotubes around the kinks. In particular, molecular dynamics (MD) simulations of individual CNTs predict that the onset of bending buckling results in a transition from quadratic to linear dependence of the bending

a)Authors to whom correspondence should be addressed. Electronic addresses: shiomi@photon.t.u-tokyo.ac.jp and lz2n@virginia.edu.

energy on the bending angle[35,36] and in a dramatic increase in the rate of the dissipation of bending oscillations.[37] The buckling kinks also hamper phonon transport along the buckled nanotubes and serve as "thermal resistors" for the heat conduction along the nanotube. A single computational study[22] investigating the thermal conductance of a buckling kink reports a value of 50 GWm^{-2} K^{-1} for the ratio of the thermal conductance of a kink in a (10,10) CNTs to the cross-sectional area of the CNT, defined in Ref. 22 as a thin shell with radius of the CNT and thickness of a single C–C bond length. One can expect that the conductance of the buckling kink varies with the degree of buckling, but this dependence has not been quantified yet.

In order to reveal the angular dependence of the conductance of the buckling kinks, we perform a series of nonequilibrium MD simulations where the thermal conductance of buckling kinks generated in an individual (10,10) single-walled CNT is evaluated for different bending angles. The results of the MD simulations are formulated in the form of a functional dependence of the thermal conductance on the buckling angle that characterizes the shape of the buckled CNT in the vicinity of the buckling kink. The predictions of the atomistic simulations are then incorporated into a mesoscopic model[32,38] developed for investigation of the effective (macroscopic) properties of CNT materials.[21] The effect of the thermal resistance of the buckling kinks on the thermal conductivity of CNT films is evaluated in mesoscopic simulations performed for films composed of nanotubes of different length, from 100 nm to 1 μm.

II. ATOMISTIC SIMULATIONS OF THERMAL CONDUCTANCE OF BUCKLING KINKS

Classical molecular dynamics (MD) simulations were carried out by modeling carbon covalent bonds of a CNT by the Tersoff-Brenner bond-order potential[39,40] with the second parameter set, which is tuned for interatomic force constants.[40] In addition, to describe the van der Waals interaction between upper and lower walls of the buckled structure, the Lennard-Jones potential,

$$\Phi_{ij} = 4\varepsilon\left[\left(\frac{\sigma}{r_{ij}}\right)^{12} - \left(\frac{\sigma}{r_{ij}}\right)^{6}\right] f_c, \tag{1}$$

was applied between ith and jth carbon atoms with parameters $\varepsilon = 2.4$ meV and $\sigma = 3.37$ Å. Here, the cutoff function was applied to the potential function as

$$f_c = \begin{cases} 1 & (d - b/2 \le r_{ij}^0 \le d + b/2) \\ 0 & \text{otherwise,} \end{cases} \tag{2}$$

where r_{ij}^0 is the equilibrium distance between ith and jth carbon atoms when the CNT is straight, $d = 1.38$ nm is the (10,10) CNT diameter, and $b = 0.34$ nm is the interlayer spacing in graphite. Thus, the atom pairs of the Lennard-Jones interaction were determined for the straight CNT and maintained throughout the bending-buckling simulation. This way, the Lennard Jones potential serves to express the van der Waals interaction between upper and lower walls of the buckled structure without noticeably altering the neighboring interatomic force constants of the graphitic network, which give reasonable phonon dispersion relations.[41]

As shown in Fig. 1(a), a buckling deformation was formed by bending a (10, 10) single-walled CNT with a length of 50.1 nm (202 unit cells). The CNT was bent by rotating the two rigid CNT ends (85 unit cells on each side) around the origin in the opposite directions to a target bending angle Θ. Here, the origin is the center of the initial straight CNT. The CNT was bent by 10^{-5} degree per time step, where the time step is 0.5 fs. The flexible part of the CNT in the middle (8-nm long, 32 unit cells) was relaxed at every time step and formed a buckling kink when the local curvature exceeded the critical value. During the bending, the distance between the end unit cell of the 8-nm-part and the origin was kept constant with the unit cell plane being orthogonal to the vector connecting the origin and the unit cell. This way, we were able to obtain a system with a local buckling kink held in the middle by two quasi-straight CNT leads. This configuration is convenient for the thermal conductance calculation since the stress resides dominantly in the buckled part.

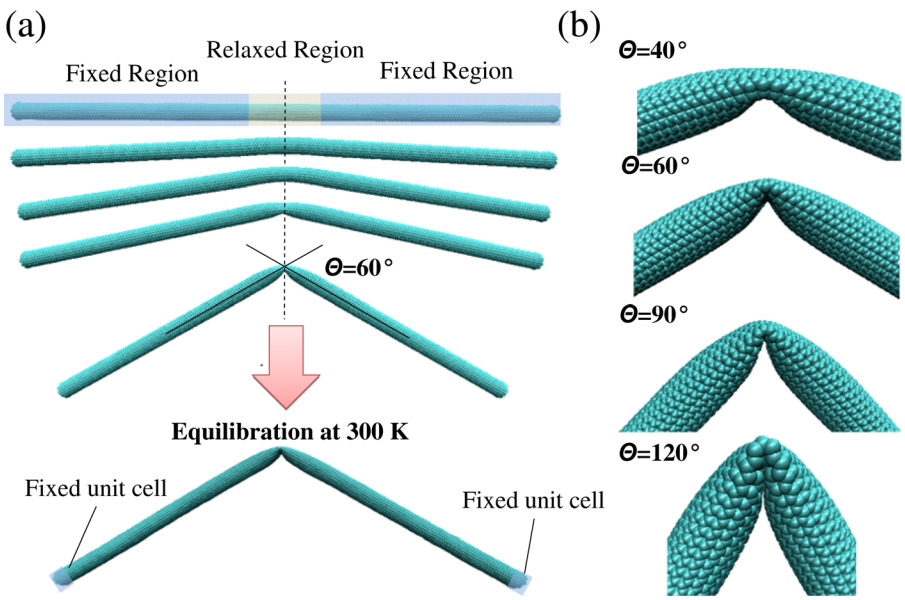

FIG. 1. (Color online) A schematic of the simulation process of bending (10, 10) CNT to a bending angle $\Theta = 60°$ (a) and snapshots of buckled structures at various values of Θ (b).

The bending simulations were performed for different bending angles Θ. After the bending simulation, as illustrated in Fig. 1(a), the buckled CNT was equilibrated at 300 K with only one unit cell at each end fixed. As shown in Fig. 1(b), the resulting buckled structures were subjected to local distortions that increased with Θ. After the equilibration, the quasi-straight parts of the CNTs deformed slightly to balance the stress at the buckled structures in the direction tangential to the fixed unit cells at the ends. Since the following mesoscopic simulations required the local angle at the buckling kink rather than the bending angle, the buckling angle[33] χ was defined and calculated as follows.

As illustrated in Fig. 2(a), the local angle Ψ is defined as the angle between the vectors P_LA_L and P_RA_R, where P and A are the positions of the centers of mass of the pth and (p-1)th unit cells, respectively. Here, the unit cell index p is counted from the center of the CNT, and the subscripts L and R denote left and right sides of the buckled CNT. When p corresponds to the end unit cells, Ψ becomes identical to Θ. With decreasing p, Ψ initially increases and subsequently decreases due to the above-mentioned deformation of the quasi-straight leads. In the close vicinity of the buckling kink (p approaches 1), Ψ increases again following the nonaxisymmetric shape of the unit cells in the buckled part of the CNT. The minimum Ψ corresponds to the angle between the ends of the buckling kink. This minimal Ψ is assumed to be equal to mesoscopic buckling angle χ, introduced in Ref. 33. With this definition, we obtained $\chi = 23.6°$, 49.5°, 82.1°, and 112.0° for $\Theta = 40.0°$, 60.0°, 90.0°, and 120.0°, respectively [Fig. 2(c)].

Thermal conductance at the buckling kink was calculated by nonequilibrium MD simulations. Temperatures of the two CNT ends were maintained at $T_C = 290$ K and $T_H = 310$ K by using the Nose-Hoover thermostat to drive a steady thermal current Q through the CNT. The length of the temperature-controlled regions was taken to be $L_{ctrl} = L/2$, where $L = 50$ nm is the thermostat-free part of the CNT. The relaxation time of the Nose-Hoover thermostat was set to be $\tau = 40$ ps. These parameters, L_{ctrl} and τ, were chosen to minimize the virtual thermal resistance between the channel and the thermostats.[42] The velocity Verlet algorithm was employed to integrate the classical Newton's equations of motion with the time step of 0.5 fs. The steady state thermal current was obtained by $Q = \langle (Q_H - Q_C)/2 \rangle$, where Q_H and Q_C are the thermal currents into the hot and cold thermostat, respectively. Then the thermal conductance of a buckling kink was calculated as $\sigma_b/A_T = Q/(A_T \Delta T)$, where ΔT is the temperature drop across the buckled structure. Here, the cross-sectional area A_T of a CNT is defined as an area of a ring with a width equal to interlayer spacing in graphite, $A_T = \pi bd$.[3]

Thermal conductance across the buckling kink exhibits strong dependence on χ as shown in Fig. 3. By fitting the dependence with a power law, we obtain

$$\sigma_b(\chi)/A_T = 636.9\chi^{-0.91}. \quad (3)$$

Hence, the thermal conductance is nearly inversely proportional to χ or, in other words, the thermal resistance is proportional to χ. The function lies close to the thermal conductance value reported by Xu and Buehler.[22] Here, the value of Xu and Buehler was rescaled to account for the difference in the definition of the tube cross section and the buckling angle was roughly estimated from the snapshot of the buckled CNT presented in Ref. 22. The obtained angular dependence of the thermal conductance (or resistance) is consistent with the work by Nishimura *et al.*,[43] who, through investigation of diameter dependence, found that the thermal resistance of the bending-induced buckling kink is proportional to the strain energy in the buckled structure. Note that the strain energy in the buckled structure is approximately proportional to the buckling angle,[30] thus explaining the approximate inverse proportionality between the buckling kink conductance and buckling angle, Eq. (3).

III. MESOSCOPIC SIMULATIONS OF THERMAL CONDUCTIVITY OF CNT FILMS

The impact of the finite thermal conductance of the buckling kinks, predicted in the atomistic simulations, on the effective thermal conductivity of CNT materials is investigated in mesoscopic modeling of thermal conductivity of

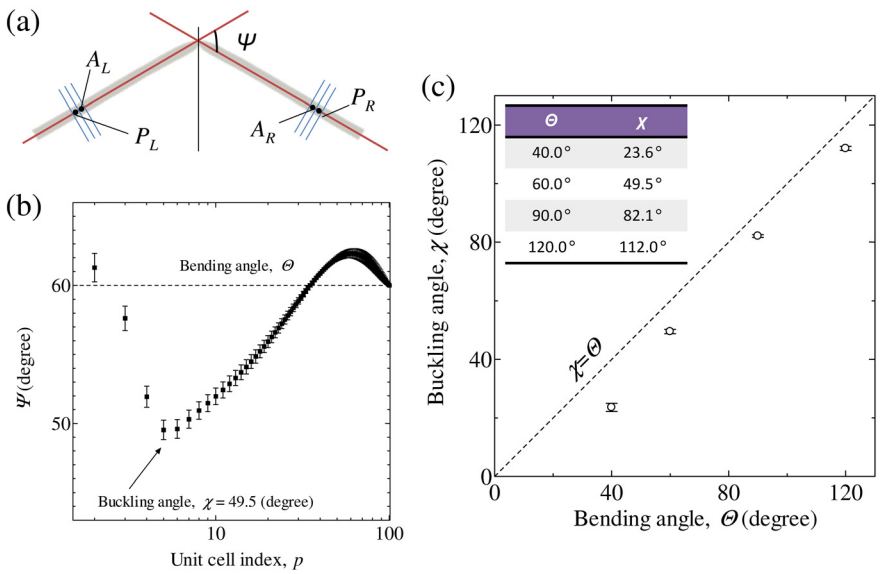

FIG. 2. (Color online) An illustration of the definition of the local angle Ψ (a), the dependence of Ψ on the unit cell index p counted from the center of the CNT (b), and the dependence of the buckling angle χ on the bending angle Θ (c). In (a), P and A are the positions of the centers of mass of pth and (p-1)th unit cells, respectively. The error bars show the standard deviation for 50 different configurations at equilibrium.

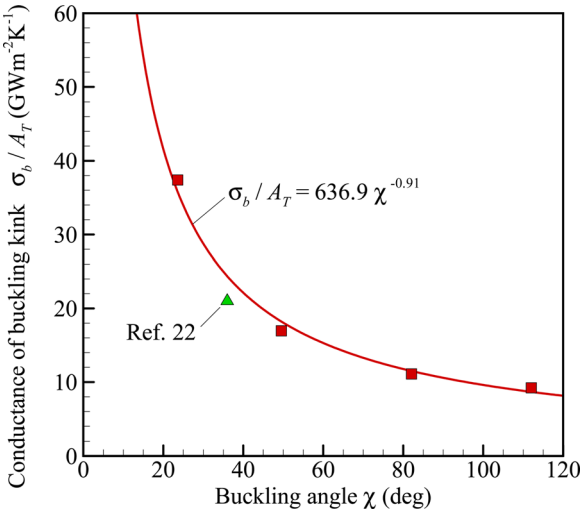

FIG. 3. (Color online) The dependence of the thermal conductance of the bending buckling kink σ_b/A_T on the buckling angle χ predicted for (10,10) CNTs in atomistic simulations. Square symbols show the values found in atomistic simulations performed in the present work and the triangle symbol shows the value recalculated from Ref. 22. Solid curve represents a power law fit to the data points given by Eq. (3).

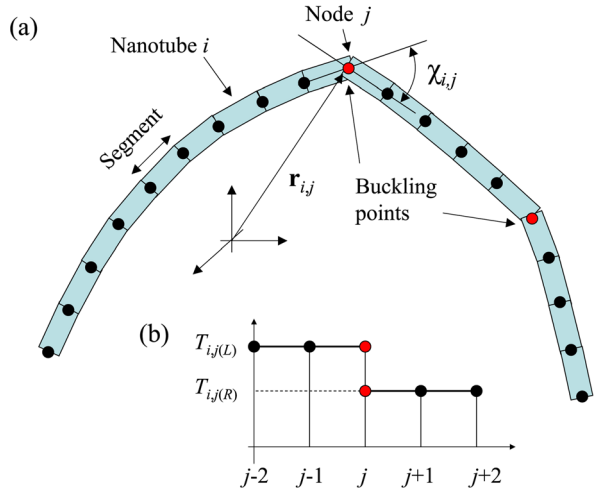

FIG. 4. (Color online) Schematic sketch of the mesoscopic representation of a nanotube i as a chain of cylindrical segments defined by nodes j (a) and the distribution of temperature along the nanotube in the vicinity of the buckling kink (b). The solid circles show the mesoscopic nodes, with nodes where buckling occurs colored red. In the mesoscopic model, the buckling angle χ_{ij} is defined as an angle between axes of segments adjacent to the buckling kink. Buckling kinks and CNT ends divide the nanotubes into several buckling-free parts. Temperature is assumed to be constant within any buckling-free part of the nanotube and exhibits a jump at buckling kinks.

CNT films. The basic principles of the dynamic mesoscopic model that enables computationally efficient simulations of self-organization of thousands of CNTs into continuous networks of bundles are briefly outlined first, in Sec. III A. The structure of CNT films is analyzed in Sec. III B and the method used for the evaluation of the thermal conductivity of the films is described in Sec. III C. The results of the calculations of thermal conductivity of the CNT films performed with both constant and buckling-angle-dependent values of the thermal conductance of the buckling kinks are presented in Sec. III D.

A. Mesoscopic modeling of the formation of CNT network materials

The mesoscopic model for simulation of CNT-based materials adopts a coarse-grained representation of individual CNTs as chains of stretchable cylindrical segments.[38] Each CNT i is defined by positions $\mathbf{r}_{i,j}$ of nodes j jointing the neighboring segments and local internal temperatures at the nodes, $T_{i,j}$, as shown in Fig. 4(a). The dynamics of a system of interacting CNTs is described by solving the equations of motion of classical mechanics for the positions of all nodes. The forces acting on the nodes are calculated based on the mesoscopic force field that includes terms describing internal stretching, bending, and buckling of nanotubes,[33,38] the van der Waals interactions among the CNTs,[32] and the interactions with external bodies.

The bending buckling of a CNT is assumed to occur at mesoscopic nodes where the local radius of curvature reaches its critical value of 27.5 nm chosen to be within the range of values predicted in quasi-static MD simulations of (10,10) CNTs.[33] In the post-buckling state, the bending energy of a part of the nanotube represented by mesoscopic segments attached to the node where the buckling occurs is described by an energy term that is proportional to the buckling angle, χ_{ij}, Fig. 4(a). The switch from the quadratic dependence on the local curvature to the linear dependence on the buckling angle represents the effective softening of the bending potential upon buckling, which is predicted in atomistic simulations.[35,36] In order to verify the agreement between the atomistic and mesoscopic models adopted in the present work, the buckling angle was calculated with the mesoscopic model applied to an individual buckled nanotube with the same computational setup used in the atomistic simulations and described in Section II. For the same bending conditions, the deviation of the buckling angles χ_{ij} predicted by the mesoscopic model from the ones computed in atomistic simulations is found to not exceed 10% for the range of angles shown in Fig. 3.

The mesoscopic model briefly described above is used to generate samples of CNT films with continuous network structures typical for real CNT materials.[32,33] The dynamic mesoscopic simulations are performed for films consisting of (10,10) single walled CNTs with length L_T varying from 100 nm to 1 μm. The films have thickness of 100 nm and material density of 0.2 g cm^{-3}, which is a typical density of CNT films and buckypaper.[25] Several simulations are also performed for films with a smaller thickness of 20 nm and only a relatively small difference from 100 nm films (below 18%) is found in the values of in-plane thermal conductivity. The initial samples used in the simulations are generated by stacking planar layers of randomly oriented and distributed straight nanotubes with a distance between the layers chosen to ensure interlayer interaction. The periodic boundary conditions are applied in the directions parallel to the film surfaces. The film density is maintained at a constant value by two planes enclosing the film from the two sides normal to the film surfaces and interacting with CNTs by a short-range repulsive potential. The equilibrium length of segments in the mesoscopic representation of CNTs is chosen to be 2 nm, more than an order of magnitude smaller than the critical

radius of curvature for the onset of bending buckling in (10,10) CNTs.

Each dynamic simulation consists of a 1 ns long constant energy part characterized by a rapid spontaneous self-assembly of CNTs into continuous networks of bundles, followed by a longer 9 – 15 ns part performed under conditions of constant 300 K temperature and characterized by slower evolution and eventual stabilization of the network structures.[32,33] The films with stable network structures of interconnected CNT bundles are produced for nanotubes with length of 150, 200, 400, and 1000 nm. A system of CNTs with length of 100 nm, which is below the critical length needed for the formation of a stable network of bundles at room temperature,[33] is also considered in the simulations. This system has a cellular structures composed of CNT bundles weakly connected with each other. While all of these films are used in the analysis of the CNT length dependence of the thermal conductivity presented in Sec. III D, two of the samples are selected for a more detailed investigation of the factors that control the heat conduction in the network structures. These are the films with $L_T = 200$ nm and dimensions of $500 \times 500 \times 100$ nm^3 (sample *A*) and $L_T = 1000$ nm and dimensions $2000 \times 2000 \times 100$ nm^3 (sample *B*).

B. Structure of CNT films

The continuous random networks of CNT bundles with partial hexagonal ordering of individual CNTs in the bundles, generated in the dynamic mesoscopic simulations, are visually similar to the structures observed in experimental images of surfaces of CNT films or "buckypaper."[24–29] In particular, the partial hexagonal ordering of individual CNTs in the bundles and the presence of multiple interconnections between bundles formed by CNTs that belong to two or more bundles simultaneously have been identified in experimental images of CNT films.[24–29] The size distributions of the CNT bundles and other structural characteristics of the network structures are determined by the length of the nanotubes and the procedure of the sample preparation (the duration of the constant energy stage of the dynamic simulations, see Sec. III A). In particular, the average number of CNTs in a bundle cross section is equal to 25.7 in sample *A* and 32.2 in sample *B*, while the mean-square deviation of the number of CNTs in a bundle cross section is close to 25 in both cases.

Both the fraction of buckled nanotubes f_b in the simulated samples and the average number of buckling kinks per buckled nanotube $\langle N_b \rangle$ increase with increasing length of the CNTs and are $f_b = 0.37$, $\langle N_b \rangle = 1.9$ in sample *A* and $f_b = 0.9$, $\langle N_b \rangle = 5$ in sample *B*, Fig. 5(a). The average number of buckling kinks per unit length of a CNT, $\langle N_b \rangle f_b / L_T$, has a weak dependence on the CNT length and is equal to 3.7 μm^{-1} in sample *A* and 4.5 μm^{-1} in sample *B*. The buckling kinks are distributed unevenly along the CNTs, with pairs or triples of buckling kinks often located close to each other, Fig. 5(b).

The mesoscopic samples can be described as networks of endless bundles that split into sub-bundles or individual CNTs, with the sub-bundles tangling and merging again into thicker bundles. The buckling kinks are mostly located in parts of nanotubes that belong to interconnections between thicker bundles, as can be seen in Fig. 5(b). The interconnections may consist of individual CNTs, but are more often (especially for samples composed of longer CNTs) represented by thinner sub-bundles that connect thicker ones. In sample *A*, which is composed of relatively short CNTs, most nanotubes belong to one or two bundles only and, thus, one can clearly distinguish nanotubes that serve as interconnections between bundles. Many of such interconnections are buckled. In samples with longer CNTs, most of the CNTs have multiple buckling kinks and simultaneously belong to several bundles. The buckling kinks in these cases are concentrated within thinner bundles that serve as interconnections between the thicker parts of the continuous network structure. Moreover, many CNTs that belong to the same interconnecting bundle tend to have buckling kinks located in a close proximity from each other.

Thus, in samples composed of sufficiently long nanotubes, most of the CNTs have multiple buckling kinks that tend to concentrate in thinner bundles serving as interconnections between the thicker bundles. The interconnections can be expected to play an important role in the heat conduction through the network structure, suggesting that the effect of the finite conductance of the buckling kinks may be amplified by the preferential buckling of the interconnections. On the other hand, as shown in Ref. 33, the statistical distribution of the buckling angles χ in samples with $L_T > 120$ nm, when the stable network of bundles is formed, is characterized by a large number of kinks with small χ. In particular, in both sample *A* and sample *B*, χ is less than 20° in more than 90% of the buckling kinks. Due to the strong dependence of σ_b on χ (see Fig. 3) and broad distributions of the buckling angles in the network structures, the quantitative effect of bending buckling on the thermal conductivity of the CNT materials is difficult to assess without direct numerical simulation of the heat flow in the mesoscopic samples.

C. Method of calculation of thermal conductivity of mesoscopic samples

The calculation of in-plane thermal conductivity k of the CNT films is performed with a method suggested in Ref. 21 and enhanced here with treatment of finite thermal conductance of the buckling kinks. Briefly, the thermal conductivity is calculated by applying a temperature gradient to a static network structure generated in a mesoscopic dynamic simulation, evaluating a steady-state heat flux through the sample, and finding the thermal conductivity from the Fourier law.

The temperature gradient is created in a mesoscopic sample by disabling the periodic boundary conditions in the x direction and cutting the CNTs that cross left-hand and right-hand sides of the sample, so that the parts of such CNTs are considered as individual nanotubes in the calculations of thermal conductivity. The mesoscopic nodes in parts of the cut nanotubes bounded by a cut segment and a buckling kink (or CNT end if no buckling kinks are present) are assigned constant temperatures T_{hot} and T_{cold} at the left-hand and right-hand sides of the sample, respectively (Fig. 6). In rare cases when the same CNT crosses the left-hand or right-hand sides

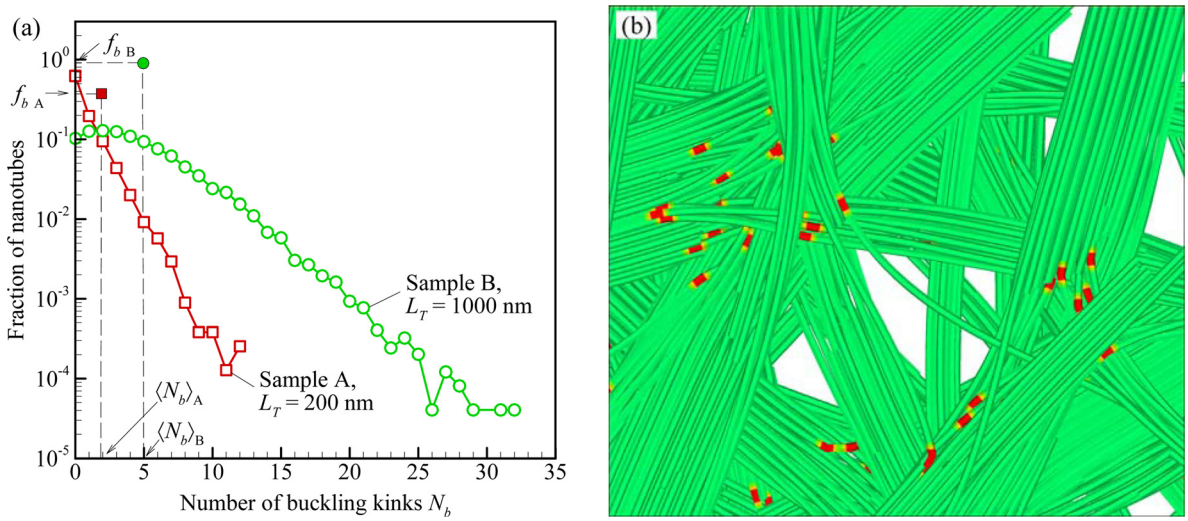

FIG. 5. (Color online) Fraction of nanotubes with a given number of buckling kinks, N_b, in samples A (red open squares) and B (green open circles) (a) and a part of sample A shown in Fig. 6 with positions of buckling kinks marked by dark (red online) color (b). The average number of buckling kinks per buckled nanotube, $\langle N_b \rangle$, and the fraction of buckled nanotubes, f_b, are marked in (a) by the solid red square and green circle for samples A and B, respectively.

of the sample more than once, the constant temperatures are also maintained for buckling-free parts of the nanotube bounded by the two cut segments. The temperatures at all nodes of all "internal" CNTs are then calculated from the balance of incoming and outgoing heat fluxes. The analysis is performed under the assumption that k is defined by the thermal resistance of the inter-tube contacts[14,17,21] and buckling kinks, whereas the intrinsic thermal resistance of individual non-buckled CNTs is neglected. That is, in a buckling kink associated with node j of nanotube i, the temperature jumps from a "left-hand side" value $T_{i,j(L)}$ to a "right-hand side" value $T_{i,j(R)}$ [Fig. 4(b)] due to the finite thermal resistance of the buckling kink, whereas in nodes representing buckling-free parts of the nanotube, $T_{i,j(L)} = T_{i,j(R)} = T_{i,j}$. With this assumption, the temperature of any buckling-free part of a nanotube, which in bounded by a CNT end and/or buckling kink(s), is constant and can be calculated from an equation expressing the balance of all incoming and outgoing heat fluxes for this part of the CNT. In particular, for a part of nanotube i bounded by buckling kinks at nodes M and N, this equation can be written as

$$Q_{b(i,M)} - Q_{b(i,N)} + \sum_{j=M}^{N-1} \sum_{k=1}^{N_T} \sum_{m=1}^{N_k-1} Q_{c(i,j)-(k,m)} = 0, \qquad (4)$$

where N_T is the total number of nanotubes in the sample, N_k is the number of mesoscopic nodes in nanotube k, $Q_{b(i,j)} = \sigma_{b(i,j)}(T_{i,j(L)} - T_{i,j(R)})$ is the heat flux through the buckling kink in node j of nanotube i, and $Q_{c(i,j)-(k,m)} = \sigma_{c(i,j)-(k,m)}(T_{i,j(R)} - T_{k,m(R)})$ is the contact heat flux between a pair of mesoscopic segments defined by nodes j and $j+1$ of nanotube i and nodes m and $m+1$ of nanotube k. The thermal conductance of a buckling kink is a function of the buckling angle, $\sigma_{b(i,j)} = \sigma_b(\chi_{i,j})$ given by Eq. (3), and the contact thermal conductance for a pair of interacting mesoscopic segments, $\sigma_{c(i,j)-(k,m)}$, is calculated as follows:[21]

$$\sigma_{c(i,j)-(k,m)} = \sigma_{c0} \frac{\Psi_{(i,j)-(k,m)}}{\Psi_0},$$
$$\Psi_{(i,j)-(k,m)} = n_\sigma^2 \int_{S_{(i,j)}} \int_{S_{(k,m)}} \psi(r) dS_{(k,m)} dS_{(i,j)}, \qquad (5)$$

where the integration is performed over the surfaces of the interacting segments, r is the distance between points on surfaces of different segments, $\psi(r)$ is a "heat transfer" function[21] that vanishes for atomic pairs with $r > r_c$ ($r_c = 10.2$ Å is the cutoff distance of the carbon-carbon interatomic potential for nonbonded interactions), Ψ_0 is a value of $\Psi_{(i,j)-(k,m)}$ for a geometrical arrangement of segments for which the conductance is known and equal to σ_{c0}, and n_σ is the surface number density of carbon atoms in the CNT. This method accounts for a continuous transition between the limiting

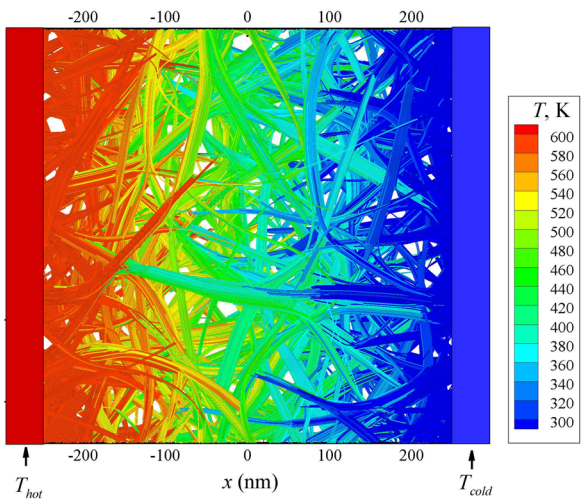

FIG. 6. (Color online) Steady-state temperature distribution established in a mesoscopic sample A and used in the calculation of the thermal conductivity of the network structure. The sample has dimensions of $500 \times 500 \times 100$ nm^3 and is composed of 7829 (10,10) CNTs with $L_T = 200$ nm and material density of 0.2 g cm^{-3}. The nanotubes are colored by their temperature. The temperature distribution is shown for $\sigma_b = \infty$, but it is visually indistinguishable from the one calculated with $\sigma_b = 0$.

cases of parallel and perpendicular CNTs that have been investigated in MD simulations[14–19] and experiments.[20] For (10,10) CNTs, the model given by Eq. (5) is parameterized by the value $\sigma_{c0} = 5 \times 10^{-11}$ WK^{-1} found in atomistic Green's function calculations for two CNTs crossing each other at a 90° angle.[14]

For buckling-free parts of CNTs bounded from one or both sides by the end(s) of the nanotube (i.e. when nodes M and/or N coincide with the end(s) of the CNT) the corresponding heat fluxes $Q_{b(i,M)}$ and/or $Q_{b(i,N)}$ are set to zero in Eq. (4). The heat balance equation is not solved for buckling-free parts of CNTs that are crossing the left-hand and right-hand sides of the sample; rather, the temperatures of all segments in these parts are fixed at the corresponding values of T_{hot} or T_{cold}.

The heat flux Q_x through any cross-section of the sample that is perpendicular to the x axis can be calculated, e.g., by evaluating the total contact heat fluxes $Q_{x(\text{cold})}$ and $Q_{x(\text{hot})}$ for CNTs that are crossing the left-hand and right-hand sides of the sample:

$$\begin{aligned} Q_{x(\text{hot})} &= \sum_{i=1}^{N_T} \sum_{j=1}^{N_i-1} \delta_{i(\text{hot})} \sum_{k=1}^{N_T} \sum_{m=1}^{N_k-1} Q_{c(i,j)-(k,m)}, \\ Q_{x(\text{cold})} &= -\sum_{i=1}^{N_T} \sum_{j=1}^{N_i-1} \delta_{i(\text{cold})} \sum_{k=1}^{N_T} \sum_{m=1}^{N_k-1} Q_{c(i,j)-(k,m)}, \end{aligned} \tag{6}$$

where $\delta_{i(\text{hot})}$ ($\delta_{i(\text{cold})}$) is equal to unity if CNT i crosses the left (right)-hand sides of the sample and is equal to zero otherwise. The heat flux $Q_x = Q_{x(\text{cold})} = Q_{x(\text{hot})}$ is determined by solving a linear system of equations given for all buckling-free parts of the CNTs by Eq. (4). The equations are solved for the nodal temperatures iteratively by the Gauss-Seidel method,[44] until the condition $2|Q_{x(\text{cold})} - Q_{x(\text{hot})}|/(Q_{x(\text{cold})} + Q_{x(\text{hot})}) < 10^{-6}$ is satisfied.

Once the heat flux Q_x and nodal temperatures of all "internal" nanotubes in the sample are calculated, the temperature gradient in the x direction, ∇T_x, is evaluated for the central part of the sample, where the distribution of the temperature is linear. The temperature gradient ∇T_x is not equal to the imposed value $(T_{\text{cold}} - T_{\text{hot}})/L_x$ (L_x is the length of the sample along the x axis) since the presence of CNT segments maintained at constant temperatures T_{hot} and T_{cold} results in a non-linear distribution of the average material temperature in the vicinities of the constant temperature sides of the sample. Finally, the in-plane thermal conductivity of the film is calculated based on the Fourier law, $k = -Q_x/(A_x \nabla T_x)$, where A_x is the area of the sample cross section in the direction perpendicular to the x axis. Since neither $\sigma_{b(i,j)}$ nor $\sigma_{c(i,j)-(k,m)}$ in Eq. (4) depends on temperature, the calculated values of k do not depends on the choice of T_{cold} and T_{hot} used in the calculations. The temperatures of $T_{\text{cold}} = 300$ K and $T_{\text{hot}} = 600$ K are specified in Fig. 6 for visualization purposes only.

D. Thermal conductivity of CNT films

In order to reveal general trends in variation of the thermal conductivity of CNT films due to the finite thermal resistance of buckling kinks, the calculations of thermal conductivity were performed for both constant values of the conductance, $\sigma_b/A_T = \text{const}$, that spans the range from 0 to 50 GWm^{-2} K^{-1} and variable angular-dependent conductance, $\sigma_b(\chi)$, defined by Eq. (3). The results of the calculations are related to the data obtained in Ref. 21 under conditions of zero thermal resistance of the buckling kinks ($\sigma_b = \infty$).

The effect of the finite values of the thermal conductance of the buckling kinks on the temperature distribution in the CNT films is found to be fairly weak in all calculations, regardless of the assumed value of σ_b. Although the calculations based on Eq. (4) assume an abrupt temperature change at any of the buckling kinks, the actual differences, $T_{i,j(L)} - T_{i,j(R)}$, appear to be relatively small even for $\sigma_b = 0$, which corresponds to buckling kinks acting as perfect thermal insulators. For instance, the temperature distribution calculated for sample A under the assumption of zero thermal resistance of the buckling kinks ($\sigma_b = \infty$) and shown in Fig. 6 is visually indistinguishable from the one calculated under the assumption of thermally insulating kinks ($\sigma_b = 0$) when the temperature scale adopted in Fig. 6 is used.

Despite the relatively weak effect on the temperature of individual CNTs, the finite thermal conductance of the buckling kinks results in non-negligible changes in the thermal conductivity of the CNT films. The results of the calculations performed with constant (angular-independent) values of the thermal conductance are shown for samples A and B in Fig. 7. For the range of values of σ_b considered in this work, the ratio of thermal conductivity k to the conductivity k_0, predicted for zero thermal resistance of the buckling kinks, is substantially smaller than unity, particularly in the case of sample B composed of longer CNTs. The thermal conductivity k increases with increasing σ_b, but remains 4% and 29% below k_0 for samples A and B, respectively, at $\sigma_b/A_T = 50$ GWm^{-2} K^{-1}.

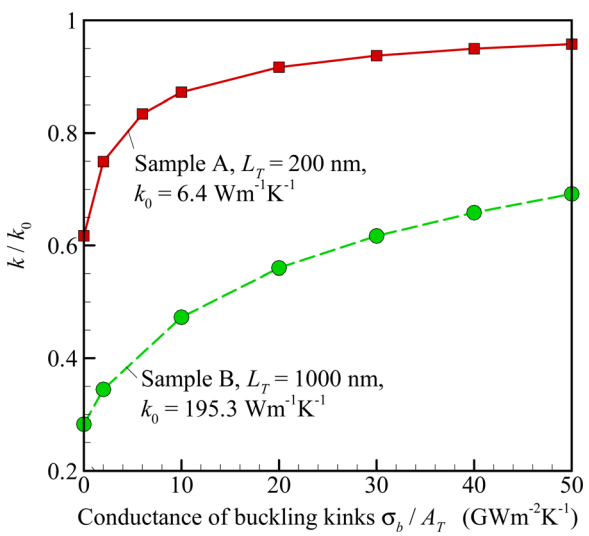

FIG. 7. (Color online) Ratio of thermal conductivity k calculated for different values of constant conductance of buckling kinks ($\sigma_b/A_T = \text{const.}$) to the thermal conductivity k_0 calculated with zero thermal resistance of buckling kinks ($\sigma_b = \infty$). The results are shown for samples A ($L_T = 200$ nm; red squares and solid curve) and B ($L_T = 1000$ nm; green circle and dashed curve).

The values of k/k_0 obtained with $\sigma_b = 0$ are equal to 0.66 and 0.31 for samples *A* and *B*, respectively. These values represent the lower bound estimates of the conductivity for an arbitrary $\sigma_b(\chi)$ dependence. The decrease of the film conductivity due to the presence of the insulating buckling kinks with $\sigma_b = 0$ has the same physical origin as the decrease in the conductivity with decreasing CNT length. A quadratic scaling of the thermal conductivity has been derived analytically for random networks of straight CNTs in which the thermal transport is controlled by the inter-tube contact resistance, while a similar superquadratic dependence ($k_0 \propto L_T^{2.2}$) is found for the networks of bundles considered in the present work under condition of $\sigma_b = \infty$.[21] The quadratic scaling, however, cannot be directly applied for the evaluation of the thermal conductivity in a film where the average length of CNTs is reduced to $L_T/(\langle N_b \rangle f_b)$ by the virtual cuts at the buckling kinks with $\sigma_b = 0$. For example, $\langle N_b \rangle f_b \approx 4.5$ for sample *B* and, hence, the expected ratio of the conductivities based on the quadratic scaling law $k_0 \propto L_T^2$ would be $k/k_0 \approx 0.05$. The actual value of k/k_0 calculated with $\sigma_b = 0$ is substantially larger, $k/k_0 \approx 0.31$. The reason for this discrepancy is in a highly uneven distribution of buckling kinks in the CNT films, with buckling kinks concentrating in bundles serving as interconnections in the network structures. Moreover, the scaling laws are derived in Ref. 21 for fixed (rather than average) length of the CNTs and should be modified for a given length distribution. It is worth noting that in a case when every nanotube in the sample *B* is virtually cut into two equal parts and the thermal resistance of the buckling kinks is neglected, the mesosopic simulation predicts roughly four-fold decrease in k_0 in agreement with the quadratic scaling law.

The preferential buckling of CNTs that belong to thin bundles serving as interconnections between thicker bundles, revealed in the structural analysis discussed in Sec. III B, suggests that the effect of buckling on the thermal conductivity of the films is largely defined by the role the interconnects play in the heat conduction through the network structures. In order to characterize the contribution of different types of structural elements of the networks to the overall heat conduction in a CNT film, we calculate the sum of absolute values of the contact heat fluxes for a given CNT *i*:

$$Q_{\Sigma(i)} = \sum_{j=1}^{N_i-1} \sum_{k=1}^{N_T} \sum_{m=1}^{N_k-1} |Q_{c(i,j)-(k,m)}|, \tag{7}$$

which is hereafter is referred to as the "total heat flux sum." A large value of $Q_{\Sigma(i)}$ indicates that nanotube *i* is an important channel of the heat conduction through the network and, therefore, $Q_{\Sigma(i)}$ can be used as a rough measure of the involvement of individual CNTs into the overall heat conduction process in the material.

The visual pictures of the distributions of $Q_{\Sigma(i)}$ in the network structures, e.g., Fig. 8, are fairly complex, but still provide opportunities for making a number of important observations. In the calculations performed with zero thermal resistance of the buckling kinks [Fig. 8(a)], thick bundles, such as a bundle marked by *BB*, are composed of CNTs with relatively small $Q_{\Sigma(i)}$, while much larger values of $Q_{\Sigma(i)}$ are characteristic for individual CNTs, thin bundles that serve as interconnections, and thick bundles that split into many sub-bundles, such as a bundle marked by *AA*. Turning the buckled segments of CNTs to thermal insulators by assuming $\sigma_b = 0$ makes almost no visible impact on the values of $Q_{\Sigma(i)}$ in thick bundles such as the *BB* one, but significantly reduces $Q_{\Sigma(i)}$ in thin bundles and split bundles such as the *AA* one [Fig. 8(b)]. These qualitative observations highlight the importance of the preferential buckling of the interconnections between bundles in defining the impact of the finite conductance of the buckling kinks on the thermal conductivity of the CNT materials.

In order to quantify the special role of the buckled interconnections in the overall heat conduction, the values of the

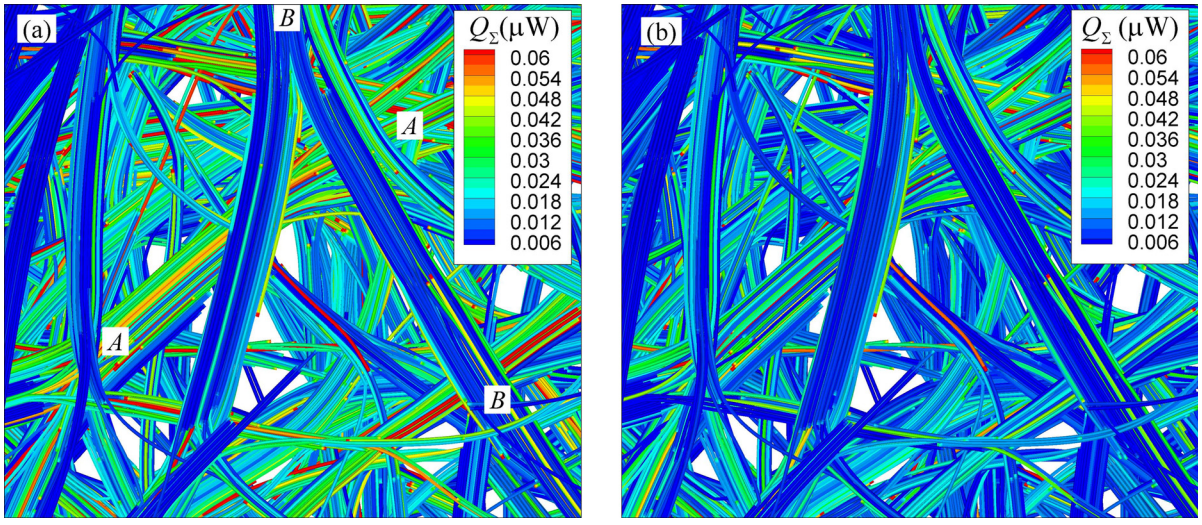

FIG. 8. (Color online) A part of sample *A* shown in Fig. 6 with nanotubes colored by their total heat flux sum $Q_{\Sigma(i)}$, Eq. (7), calculated with $\sigma_b = \infty$ (a) and $\sigma_b = 0$ (b). *AA* and *BB* mark two characteristic bundles of CNTs. Bundle *AA* splits into many thinner bundles and includes multiple buckled CNTs. As a result, the values of $Q_{\Sigma(i)}$ for nanotubes in this bundle are visibly different in panels (a) and (b). Bundle *BB* mostly consists of nonbuckled CNTs, and the values of $Q_{\Sigma(i)}$ for nanotubes in this bundle exhibit only small difference between panels (a) and (b).

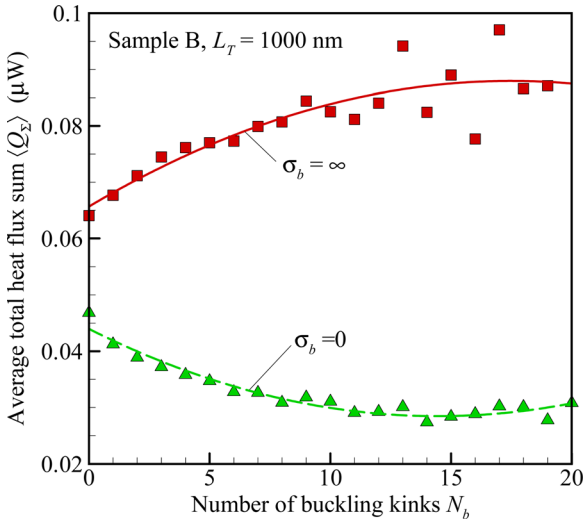

FIG. 9. (Color online) The values of the total heat flux sum $Q_{\Sigma(i)}$ averaged over individual nanotubes that have the same number of buckling kinks N_b. The results are calculated for sample B with $\sigma_b = \infty$ (red squares) and $\sigma_b = 0$ (green triangles). Data for $N_b > 15 - 20$ exhibit strong scattering due to the small number of corresponding nanotubes in the sample. The curves show least-squares quadratic polynomial approximation of data points with $N_b \leq 20$.

total heat flux sum are averaged over nanotubes with the same number of buckling kinks, N_b, and the dependence of the average quantities $\langle Q_\Sigma \rangle$ on N_b are shown for sample B in Fig. 9. The values of $\langle Q_\Sigma \rangle$ calculated with $\sigma_b = \infty$ increase with increasing N_b, indicating that CNTs that contain a larger number of buckling kinks are, on average, more active participants of the heat conduction than CNTs with smaller number of buckling kinks. As discussed in Sec. III B, the CNTs with large numbers of buckling kinks are also the ones that buildup the interconnections in the network structures of the films. It is not surprising, then, that when the buckling kinks are assumed to be thermally insulating ($\sigma_b = 0$), an opposite trend of $\langle Q_\Sigma \rangle$ decreasing with N_b is observed. In this case, the maximum $\langle Q_\Sigma \rangle$ corresponds to buckling-free CNTs, because all other CNTs are virtually cut and cannot efficiently participate in the heat conduction. It is remarkable, though, that the presence of thermally insulating buckling kinks significantly reduces $\langle Q_\Sigma \rangle$ even for the buckling-free CNTs. The dependences of $\langle Q_\Sigma \rangle$ on N_b in sample A with much shorter CNTs is qualitatively similar to the ones shown in Fig. 9.

The results of the calculations of the thermal conductivity k performed with the variable angular-dependent thermal conductance, $\sigma_b(\chi)$, predicted in the atomistic simulations and defined by Eq. (3), are shown in Fig. 10 for samples composed of CNTs of various length. The deviation of k from values obtained in calculations where the thermal resistance of the buckling kinks is neglected increases with increasing length of the CNTs. The deviation, however, is smaller than the one of values obtained in calculations performed with the highest constant value of the thermal conductance ($\sigma_b/A_T = 50$ GWm^{-2} K^{-1}). In particular, the thermal conductivity of sample B is only about 21% below the value calculated with $\sigma_b = \infty$. The relatively weak effect of the thermal resistance of the buckling kinks on k can be explained by the fact that most of the buckling angles in the network structures are small[33] and the corresponding values of the conductance predicted with Eq. (3) are high. In particular, the mean and most probable values of σ_b/A_T evaluated for sample B from the probability density function shown in Fig. 11 are on the order of 100 WGm^{-2} K^{-1}, which, according to Eq. (3), corresponds to the conductance at a buckling angle of about 7.6°. The broad distribution of the values of the thermal conductance of the buckling kinks highlights the importance of using a realistic angular dependence of the conductance in calculations that aim at an accurate quantitative description of the thermal conductivity of CNT

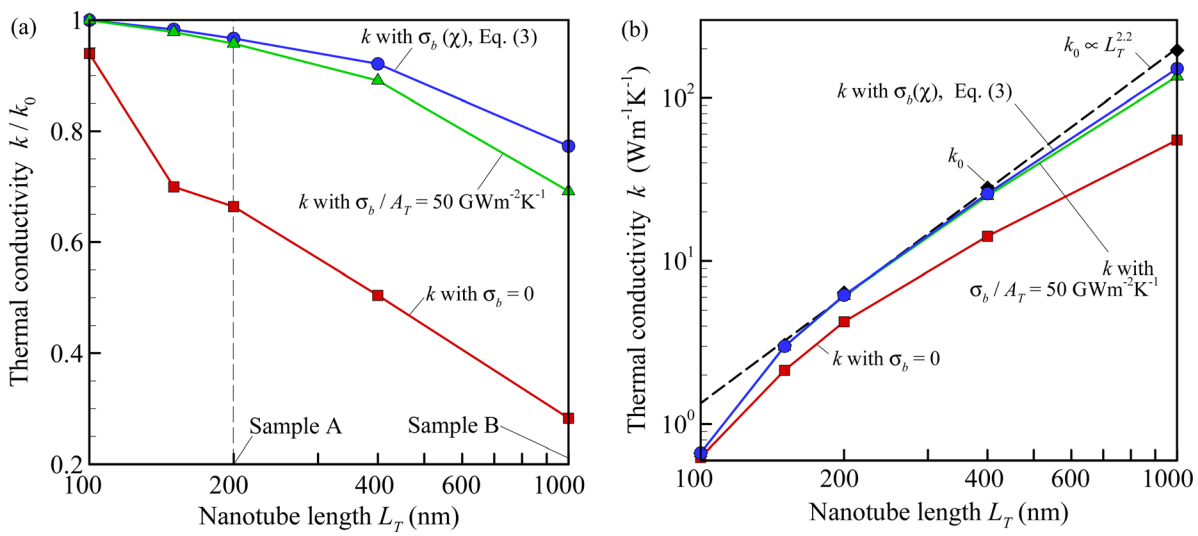

FIG. 10. (Color online) The results of the calculation of thermal conductivity k performed for mesoscopic samples composed of nanotubes of different length with constant values of thermal conductance of the buckling kinks (red squares for $\sigma_b = 0$ and green triangles for $\sigma_b/A_T = 50$ GWm^{-2} K^{-1}) and with angular-dependent thermal conductance $\sigma_b(\chi)$ given by Eq. (3) (blue circles). The data in (a) are normalized to the thermal conductivity k_0 predicted for zero resistance of the buckling kinks ($\sigma_b = \infty$). In panel (b), the corresponding dimensional values of k and k_0 are plotted. The black dashed line in (b) shows the approximate scaling law $k_0 \propto L_T^{2.2}$ obtained in Ref. 21 for the $k_0(L_T)$ dependence. The values of k_0 shown by diamonds in (b) are slightly different from the ones in Ref. 21 because of a small difference in the methods used in the calculations of the temperature gradient ∇T_x.

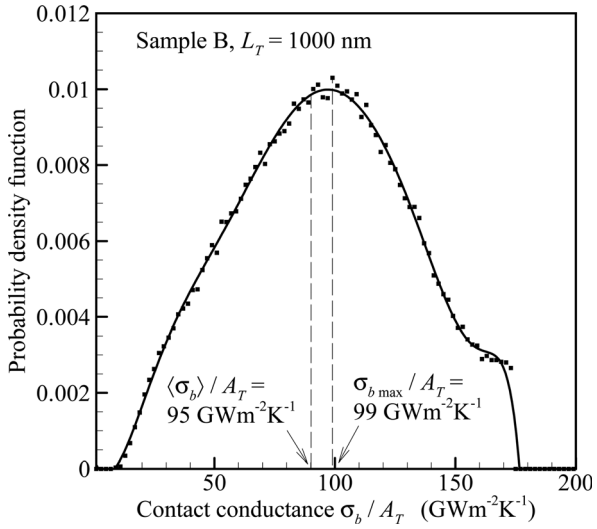

FIG. 11. Probability density function of the thermal conductance of the buckling kinks σ_b/A_T in sample B ($L_T = 1000$ nm) calculated with the angular dependence of the conductance on the buckling angle, $\sigma_b(\chi)$, given by Eq. (3). The dots show the values obtained from the actual distribution of the buckling angles and the curve is least-squares 10th order polynomial approximation of the data points with $\sigma_b/A_T \leq 177$ GWm^{-2} K^{-1}. $\sigma_{b\,max}$ and $\langle\sigma_b\rangle$ are the most probable and mean values of the conductance σ_b.

materials. The effect of the buckling kinks increases with increasing length of the nanotubes. For longer CNTs, however, the increasing contribution of the intrinsic thermal resistance of the nanotubes, not included in the present mesoscopic calculations, may overshadow the contribution of the buckling kinks. Indeed, the reduction of the thermal conductivity of the films as a result of the inclusion of the finite intrinsic conductivity of the CNTs is found to be larger than the reduction due to the buckling kinks [with angular-dependent conductance of Eq. (3)] for all samples considered in the mesoscopic calculations even if a relatively large intrinsic conductivity of 2000 Wm^{-1} K^{-1} is assumed in the calculations.

IV. SUMMARY

The results of non-equilibrium molecular dynamics simulations of heat conduction in (10,10) single-walled carbon nanotubes reveal a strong dependence of the thermal conductance of a buckling kink σ_b on the buckling angle. For a range of buckling angles from 20° to 110° the values of σ_b/A_T vary from 40 to 10 GWm^{-2} K^{-1} which agree by the order of magnitude with the value reported in an earlier study.[22] The implications of the finite thermal conductance of the buckling kinks on the conductivity of CNT-based materials are investigated in mesoscopic calculations performed for CNT films composed of thousands of CNTs arranged into continuous networks of bundles. The mesoscopic calculations are performed for several constant values of the thermal conductance of the buckling kinks, as well as for the angular-dependent conductance predicted in the atomistic simulations. The results of the calculations suggest that the buckling kinks make a moderate, but not negligible, contribution to the thermal conductivity of CNT-based materials and the account for the angular dependence of the thermal conductance of the buckling kinks is essential for accurate quantitative evaluation of the thermal conductivity. The effect of the finite buckling conductance on the thermal conductivity of the network structures is amplified by the preferential buckling of thin bundles and individual CNTs serving as interconnections between thicker bundles in the network structures. The total heat flux passing through the CNTs that are parts of the interconnections is, on average, higher than in other parts of the network structures. Consequently, the high concentration of the buckling kinks in interconnects results in a stronger impact of the buckling on the overall thermal conductivity of the films. The effect of the buckling kinks on the thermal conductivity of the CNT films increases with increasing length of the nanotubes and accounts for about 20% reduction of the conductivity of a film composed of 1 μm long CNTs. The method developed in this work for the investigation of the effect of buckling kinks on the heat conduction in CNT materials can be readily extended to systems with various types of structural imperfections that can be described in terms of the effective "conductance" of the defected CNT regions.

ACKNOWLEDGMENTS

A.N.V., D.N., and L.V.Z. acknowledge financial support by AFOSR (Grant FA9550-10-10545) and NSF (Grant CBET-1033919), as well as computational support by NSF through TeraGrid resources (project TG-DMR110090) and NCCS at ORNL, USA (project MAT009). T.S. and J.S. acknowledge partial support by KAKENHI 23760178 and 22226006, and Global COE program, "Global Center of Excellence for Mechanical System Innovation" from the Ministry of Education, Culture, Sports, Science and Technology of Japan.

[1]J. Che, T. Cağin, and W. A Goddard III, Nanotechnology **11**, 65 (2000).
[2]S. Berber, Y.-K. Kwon, and D. Tománek, Phys. Rev. Lett. **84**, 4613 (2000).
[3]S. Maruyama, Physica B **323**, 193 (2002).
[4]G. Zhang and B. Li, J. Chem. Phys. **123**, 114714 (2005).
[5]R.-Q. Pan, Z.-J. Xu, and Z.-Y. Zhu, Chin. Phys. Lett. **24**, 1321 (2007).
[6]P. Kim, L. Shi, A. Majumdar, and P. L. McEuen, Phys. Rev. Lett. **87**, 215502 (2001).
[7]M. Fujii, X. Zhang, H. Xie, H. Ago, K. Takahashi, T. Ikuta, H. Abe, and T. Shimizu, Phys. Rev. Lett. **95**, 065502 (2005).
[8]E. Pop, D. Mann, Q. Wang, K. Goodson, and H. Dai, Nano Lett. **6**, 96 (2006).
[9]A. A. Balandin, Nature Mater. **10**, 569 (2011).
[10]J. Hone, M. C. Llaguno, N. M. Nemes, A. T. Johnson, J. E. Fischer, D. A. Walters, M. J. Casavant, J. Schmidt, and R. E. Smalley, Appl. Phys. Lett. **77**, 666 (2000).
[11]P. Gonnet, Z. Liang, E. S. Choi, R. S. Kadambala, C. Zhang, J. S. Brooks, B. Wang, and L. Kramer, Curr. Appl. Phys. **6**, 119 (2006).
[12]I. Ivanov, A. Puretzky, G. Eres, H. Wang, Z. Pan, H. Cui, R. Jin, J. Howe, and D. B. Geohegan, Appl. Phys. Lett. **89**, 223110 (2006).
[13]M. E. Itkis, F. Borondics, A. Yu, and R. C. Haddon, Nano Lett. **7**, 900 (2007).
[14]R. S. Prasher, X. J. Hu, Y. Chalopin, N. Mingo, K. Lofgreen, S. Volz, F. Cleri, and P. Keblinski, Phys. Rev. Lett. **102**, 105901 (2009).
[15]H. Zhong and J. R. Lukes, Phys. Rev. B **74**, 125403 (2006).
[16]S. Maruyama, Y. Igarashi, Y. Taniguchi, and J. Shiomi, J. Thermal Sci. Technol. **1**, 138 (2006).
[17]Y. Chalopin, S. Volz, and N. Mingo, J. Appl. Phys. **105**, 084301 (2009).

[18]Z. Xu and M. J. Buehler, ACS Nano **3**, 2767 (2009).
[19]V. Varshney, S. S. Patnaik, A. K. Roy, and B. L. Farmer, J. Phys. Chem. C **114**, 16223 (2010).
[20]J. Yang, S. Waltermire, Y. Chen, A. A. Zinn, T. T. Xu, and D. Li, Appl. Phys. Lett. **96**, 023109 (2010).
[21]A. N. Volkov and L. V. Zhigilei, Phys. Rev. Lett. **104**, 215902 (2010).
[22]Z. Xu and M. J. Buehler, Nanotechnology **20**, 185701 (2009).
[23]T. Yamamoto and K. Watanabe, Phys. Rev. Lett. **96**, 255503 (2006).
[24]A. Thess, R. Lee, P. Nikolaev, H. Dai, P. Petit, J. Robert, C. Xu, Y. H. Lee, S. G. Kim, A. G. Rinzler, D. T. Colbert, G. E. Scuseria, D. Tománek, J. E. Fischer, and R. E. Smalley, Science **273**, 483 (1996).
[25]A. G. Rinzler, J. Liu, H. Dai, P. Nikolaev, C. B. Huffman, F. J. Rodríguez-Macías, P. J. Boul, A. H. Lu, D. Heymann, D. T. Colbert, R. S. Lee, J. E. Fischer, A. M. Rao, P. C. Eklund, and R. E. Smalley, Appl. Phys. A: Mater. Sci. Process. **67**, 29 (1998).
[26]F. Hennrich, S. Lebedkin, S. Malik, J. Tracy, M. Barczewski, H. Rösner, and M. Kappes, Phys. Chem. Chem. Phys. **4**, 2273 (2002).
[27]T. V. Sreekumar, T. Liu, S. Kumar, L. M. Ericson, R. H. Hauge, and R. E. Smalley, Chem. Mater. **15**, 175 (2003).
[28]L. Berhan, Y. B. Yi, A. M. Sastry, E. Munoz, M. Selvidge, and R. Baughman, J. Appl. Phys. **95**, 4335 (2004).
[29]S. Wang, Z. Liang, B. Wang, and C. Zhang, Adv. Mater. **19**, 1257 (2007).
[30]S. Iijima, C. Brabec, A. Maiti, and J. Bernholc, J. Chem. Phys. **104**, 2089 (1996).
[31]Z. R. Abrams and Y. Hanein, J. Phys. Chem. B **110**, 21419 (2006).
[32]A. N. Volkov and L. V. Zhigilei, J. Phys. Chem. C **114**, 5513 (2010).
[33]A. N. Volkov and L. V. Zhigilei, ACS Nano **4**, 6187 (2010).
[34]B. I. Yakobson, C. J. Brabec, and J. Bernholc, Phys. Rev. Lett. **76**, 2511 (1996).
[35]J. Zhu, Z. Y. Pan, Y. X. Wang, L. Zhou, and Q. Jiang, Nanotechnology **18**, 275702 (2007).
[36]G. Cao and X. Chen, Phys. Rev. B **73**, 155435 (2006).
[37]W. Jacobs, D. Nicholson, A. N. Volkov, and L. V. Zhigilei (in preparation).
[38]L. V. Zhigilei, C. Wei, and D. Srivastava, Phys. Rev. B **71**, 165417 (2005).
[39]J. Tersoff, Phys. Rev. B **37**, 6991 (1988).
[40]D. W. Brenner, Phys. Rev. B **42**, 9458 (1990).
[41]J. Shiomi and S. Maruyama, Phys. Rev. B **73**, 205420 (2006).
[42]J. Shiomi and S. Maruyama, Jpn. J. Appl. Phys. **47**, 2005 (2008).
[43]F. Nishimura, T. Shiga, S. Maruyama, K. Watanabe, and J. Shiomi, Jpn. J. Appl. Phys. **51**, 015102 (2012).
[44]S. V. Patankar, *Numerical Heat Transfer and Fluid Flow* (Hemisphere, New York, 1980).